Methods

Plant materials

Plants were grown in the greenhouse or in the field under standard conditions. We used the B73 wild-type line. For cytokinin induction experiments, 2-week-old seedlings were excised at the shoot–root junction, and stood in water supplemented with different concentrations of cytokinin. After treatments, the seedlings were dissected into a shoot fraction (apical and axillary shoot meristems, stem and 4–5 young leaf primordia) or a leaf fraction (expanding and mature leaves). For embryo culture experiments, pollinated ears at either 13 days after pollination (first leaf stage) or 16 days after pollination (second to third leaf stage) were sterilized in 30% commercial bleach solution for 20 min then rinsed five times with sterile water. The embryos were dissected out and cultured on maize embryo culture medium (1 × Murashige and Skoog salts, 1 × Gamborg's vitamins, 2% sucrose, 0.7% agar, pH 5.7) in some cases with the addition of cytokinin (kinetin, 10^{-5}, 10^{-6} or 10^{-7} M). The embryos were cultured at 28 °C in the dark for 5–7 days then fixed and cleared and the shoot meristems were measured as described[5].

Molecular biology

Standard protocols were used for maize DNA isolation and Southern blotting[30]. For RT–PCR analysis, poly(A^+) RNA was isolated using an Oligotex messenger RNA mini kit (Qiagen) according to the manufacturer's protocol. The primers ZmRR3f (GATGGCGAGCCGCAAGTGT) and ZmRR3r (AATGCCGCTGCTACAGCTACCA) were used to amplify *ABPH1* transcripts using the one step RT–PCR kit (Qiagen). The control primers Ubi 5′ (TAAGCTGCCGATGTGCCTGCGTCG) and Ubi 3′ (CTGAAAGACAGAACATAATGAGCACAG) were used to amplify control ubiquitin transcripts. PCR conditions were 94 °C, 15 s, 62 °C, 15 s, 72 °C, 45 s, with a 1 °C reduction in annealing temperature per cycle, touching down at 56 °C annealing, followed by 15 additional cycles. The PCR cycle number was limited to ensure semi-quantitative amplification, and no PCR product was visible on the ethidium-bromide-stained agarose gels. The gels were Southern blotted and probed with an *ABPH1* or *UBIQUITIN* probe. *ABPH1* transcript levels were estimated using a phosphoimager (Fuji) and were normalized against the respective ubiquitin values. *In situ* hybridizations were performed as described[5].

Received 25 April; accepted 22 June 2004; doi:10.1038/nature02778.

1. Jean, R. *Phyllotaxis: A Systemic Study in Plant Morphogenesis* (Cambridge Univ. Press, Cambridge, UK, 1994).
2. Kuhlemeier, C. & Reinhardt, D. Auxin and phyllotaxis. *Trends Plant Sci.* **6,** 87–189 (2001).
3. Klar, A. Fibonacci's flowers. *Nature* **417,** 595 (2002).
4. Reinhardt, D. *et al.* Regulation of phyllotaxis by polar auxin transport. *Nature* **426,** 255–260 (2003).
5. Jackson, D. & Hake, S. Control of phyllotaxy in maize by the *ABPHYL1* gene. *Development* **126,** 315–323 (1999).
6. Skoog, F. & Miller, C. O. Chemical regulation of growth and organ formation in plant tissues cultured *in vitro*. *Symp. Soc. Exp. Biol.* **11,** 118–131 (1957).
7. Mok, D. W. & Mok, M. C. Cytokinin metabolism and action. *Annu. Rev. Plant Physiol. Plant Mol. Biol.* **52,** 89–118 (2001).
8. Sheen, J. Phosphorelay and transcription control in cytokinin signal transduction. *Science* **296,** 1650–1652 (2002).
9. Hutchison, C. E. & Kieber, J. J. Cytokinin signaling in *Arabidopsis*. *Plant Cell* **14** (suppl.), S47–S59 (2002).
10. Lohrmann, J. *et al.* The response regulator ARR2: a pollen-specific transcription factor involved in the expression of nuclear genes for components of mitochondrial complex I in *Arabidopsis*. *Mol. Genet. Genom.* **265,** 2–13 (2001).
11. Hwang, I. & Sheen, J. Two-component circuitry in *Arabidopsis* cytokinin signal transduction. *Nature* **413,** 383–389 (2001).
12. Sakai, H. *et al.* ARR1, a transcription factor for genes immediately responsive to cytokinins. *Science* **294,** 1519–1521 (2001).
13. To, J. P. C. *et al.* Type-A *Arabidopsis* response regulators are partially redundant negative regulators of cytokinin signaling. *Plant Cell* **16,** 658–671 (2004).
14. Greyson, R. I., Walden, D. B., Hume, J. A. & Erickson, R. O. The ABPHYL syndrome in *Zea mays*. II. Patterns of leaf initiation and the shape of the shoot meristem. *Can. J. Bot.* **56,** 1545–1550 (1978).
15. Robertson, D., Stinard, P. & Maguire, M. Genetic evidence of Mutator-induced deletions in the short arm of chromosome 9 of maize. II. wd deletions. *Genetics* **136,** 1143–1149 (1994).
16. Asakura, Y. *et al.* Molecular characterization of His-Asp phosphorelay signaling factors in maize leaves: Implications of the signal divergence by cytokinin-inducible response regulators in the cytosol and the nuclei. *Plant Mol. Biol.* **52,** 331–341 (2003).
17. Falke, J., Bass, R., Butler, S., Cherviotz, S. & Danielson, M. The two component signaling pathway of bacterial chemotaxis. *Annu. Rev. Cell Dev. Biol.* **13,** 437–512 (1997).
18. Jackson, D., Veit, B. & Hake, S. Expression of maize *KNOTTED1* related homeobox genes in the shoot apical meristem predicts patterns of morphogenesis in the vegetative shoot. *Development* **120,** 405–413 (1994).
19. D'Agostino, I. B., Deruere, J. & Kieber, J. J. Characterization of the response of the *Arabidopsis* response regulator gene family to cytokinin. *Plant Phys.* **124,** 1706–1717 (2000).
20. Che, P., Gingerich, D. J., Lall, S. & Howell, S. H. Global and hormone-induced gene expression changes during shoot development in *Arabidopsis*. *Plant Cell* **14,** 2771–2785 (2002).
21. Brandstatter, I. & Kieber, J. J. Two genes with similarity to bacterial response regulators are rapidly and specifically induced by cytokinin in *Arabidopsis*. *Plant Cell* **10,** 1009–1019 (1998).
22. Sakakibara, H. *et al.* A response-regulator homologue possibly involved in nitrogen signal transduction mediated by cytokinin in maize. *Plant J.* **14,** 337–344 (1998).
23. Taniguchi, M. *et al.* Expression of *Arabidopsis* response regulator homologs is induced by cytokinins and nitrate. *FEBS Lett.* **429,** 259–262 (1998).
24. Werner, T., Motyka, V., Strnad, M. & Schmèulling, T. Regulation of plant growth by cytokinin. *Proc. Natl Acad. Sci. USA* **98,** 10487–10492 (2001).
25. Chaudhury, A. M., Letham, S., Craig, S. & Dennis, E. S. Amp1—a mutant with high cytokinin levels and altered embryonic pattern, faster vegetative growth, constitutive photomorphogenesis and precocious flowering. *Plant J.* **4,** 907–916 (1993).
26. Helliwell, C. A. *et al.* The *Arabidopsis* AMP1 gene encodes a putative glutamate carboxypeptidase. *Plant Cell* **13,** 2115–2125 (2001).
27. Schwabe, W. W. in *Positional Controls In Plant Development* (eds Barlow, P. W. & Carr, D. J.) (Cambridge Univ. Press, 1984).
28. Callos, J. D. & Medford, J. I. Organ positions and pattern formation in the shoot apex. *Plant J.* **6,** 1–7 (1994).
29. Green, P. B. Connecting gene and hormone action to form, pattern and organogenesis; biophysical transductions. *J. Exp. Bot.* **45,** 1775–1788 (1994).
30. Taguchi-Shiobara, F., Yuan, Z., Hake, S. & Jackson, D. The *FASCIATED EAR2* gene encodes a leucine-rich repeat receptor-like protein that regulates shoot meristem proliferation in maize. *Genes Dev.* **15,** 2755–2766 (2001).

Supplementary Information accompanies the paper on **www.nature.com/nature**.

Acknowledgements We thank V. Chandler for *Spm* transposon lines, and members of the Jackson laboratory, C. Kidner, E. Vollbrecht and P. Sherwood, for comments on the manuscript. We also thank Z. Yuan and M. Krishnaswami for assistance with genetic screens, DNA isolations and Southern blotting, and T. Mulligan for help with plant propagation. Funding from the National Science Foundation (Plant and Animal Developmental Mechanisms) is also acknowledged.

Competing interests statement The authors declare that they have no competing financial interests.

Correspondence and requests for materials should be addressed to D.J. (jacksond@cshl.edu).

Suppression of anoikis and induction of metastasis by the neurotrophic receptor TrkB

Sirith Douma[1], Theo van Laar[1], John Zevenhoven[1], Ralph Meuwissen[1], Evert van Garderen[2] & Daniel S. Peeper[1]

[1]*Division of Molecular Genetics, and* [2]*Department of Experimental Animal Pathology, The Netherlands Cancer Institute, Plesmanlaan 121, Amsterdam 1066 CX, The Netherlands*

Metastasis is a major factor in the malignancy of cancers, and is often responsible for the failure of cancer treatment. Anoikis (apoptosis resulting from loss of cell–matrix interactions) has been suggested to act as a physiological barrier to metastasis; resistance to anoikis may allow survival of cancer cells during systemic circulation, thereby facilitating secondary tumour formation in distant organs[1–3]. In an attempt to identify metastasis-associated oncogenes, we designed an unbiased, genome-wide functional screen solely on the basis of anoikis suppression. Here, we report the identification of TrkB, a neurotrophic tyrosine kinase receptor[4,5], as a potent and specific suppressor of caspase-associated anoikis of non-malignant epithelial cells. By activating the phosphatidylinositol-3-OH kinase/protein kinase B pathway, TrkB induced the formation of large cellular aggregates that survive and proliferate in suspension. In mice, these cells formed rapidly growing tumours that infiltrated lymphatics and blood vessels to colonize distant organs. Consistent with the ability of TrkB to suppress anoikis, metastases—whether small vessel infiltrates or large tumour nodules—contained very few apoptotic cells. These observations demonstrate the potent oncogenic effects of TrkB and uncover a specific pro-survival function that may contribute to its metastatic capacity, providing a possible explanation for the aggressive nature of human tumours that overexpress TrkB.

To perform a functional screen for suppressors of anoikis, we selected rat intestinal epithelial (RIE) cells owing to their non-malignancy and high sensitivity to anoikis (refs 6, 7; see below). Anoikis can be induced *in vitro* by transferring epithelial cells from standard, adhesive cell culture dishes (with a hydrophilic surface that supports cell attachment and spreading) to ultra-low cluster (ULC) plates with a covalently bound hydrogel layer that effectively inhibits cellular attachment. Shifting RIE cells from adhesive to ULC dishes resulted in massive cell death (Fig. 1a, left), which was critical in view of the desired minimal number of surviving 'background' cells that would represent false positives in the screen. In agreement with previous results[7], oncogenic Ras^{V12} protein effectively suppressed anoikis (Fig. 1a, right).

Upon retroviral delivery of a high-complexity pEYK retroviral complementary DNA library[8], cells were brought into suspension and screened for surviving clones (Fig. 1b). Relative to control green fluorescent protein (GFP)-infected cells that died, a proportion of library-infected pools showed surviving clones (see Methods), including 'ME-3'; this clone effectively suppressed anoikis and formed large, spheroid aggregates in suspension (Fig. 1c). Isolation and sequencing of its proviral insert revealed a full-length, wild-type cDNA encoding TrkB, a neurotrophic tyrosine kinase receptor that is required for the ontogeny, function and survival of the mammalian nervous system[4,5] and other cell types[9–12]. Interestingly, neurite development and outgrowth may represent processes that particularly rely on adhesion-independent survival[13].

To characterize the biological effects of TrkB, we generated, by retroviral delivery, pools of epithelial cells stably expressing TrkB, its primary ligand (brain-derived neurotrophic factor (BDNF))[14,15], or both (Supplementary Fig. S1a). On adhesive plates, TrkB, but not BDNF, disrupted epithelial cell organization, which was aggravated by ligand co-expression, resulting in complete loss of cell–cell contact and, upon reaching confluency, in continued proliferation as spheroids in suspension (Fig. 1d, Supplementary Fig. S1b, c).

To confirm that TrkB suppresses anoikis, we followed the fate of TrkB-expressing epithelial cells in suspension. In ULC dishes, both empty-vector and BDNF-expressing cells underwent cell death, starting at day two and leaving no surviving cells after two weeks (Fig. 1e). By contrast, TrkB effectively suppressed cell death and allowed cells to proliferate as large spheroid aggregates in suspension, explaining the identification of TrkB in the screen. Co-expression of TrkB with BDNF led to a further increase in cell number (Supplementary Fig. S1d). Similar results were obtained for murine and human epithelial cells (Supplementary Fig. S1e). The observation that the entire polyclonal TrkB-expressing cell population was resistant to anoikis argued against clonal events being due to genetic mutations. This was further supported by a soft-agar assay, which reinforced our notion that TrkB expression bypasses the need for anchorage, with virtually every TrkB-expressing cell producing a colony (Fig. 1f).

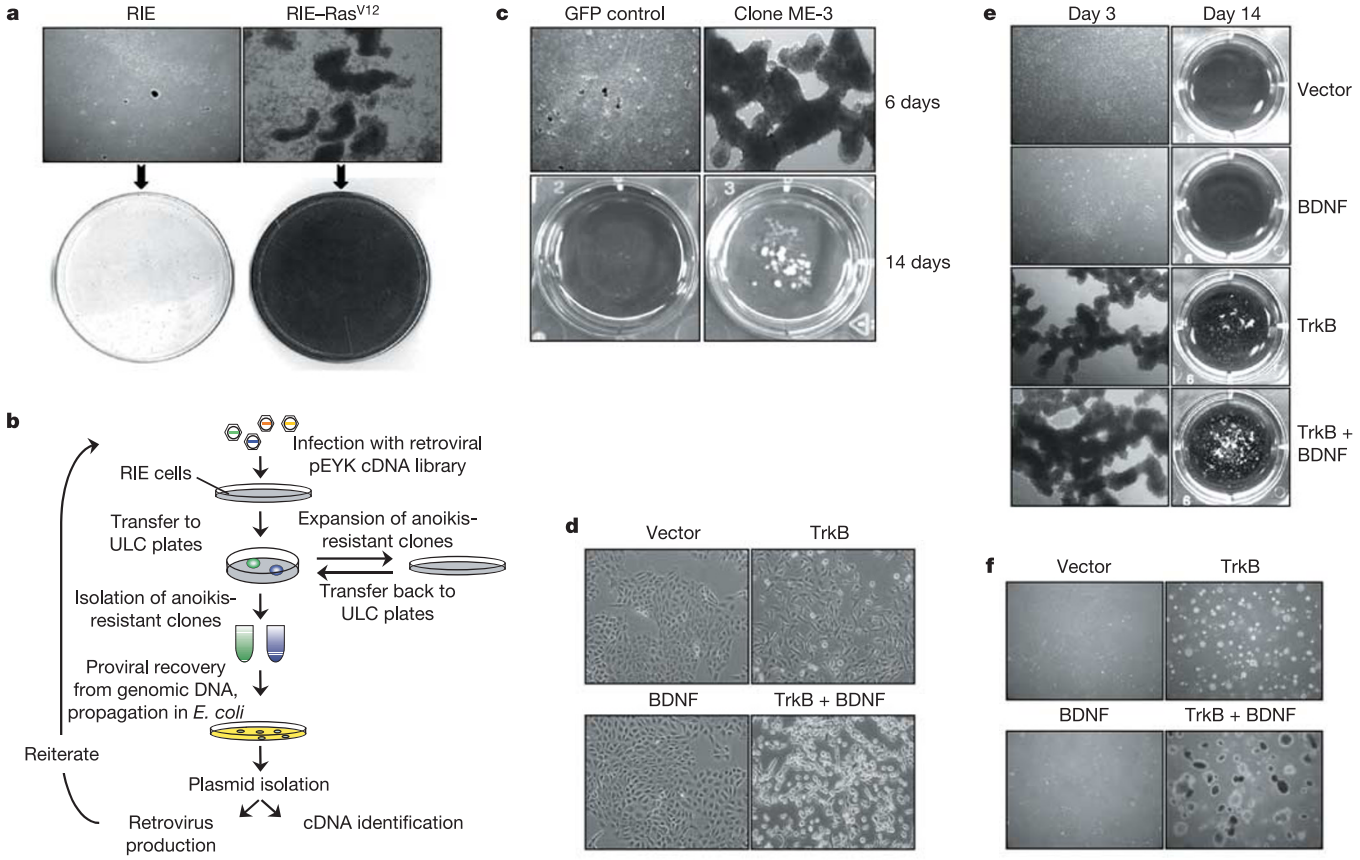

Figure 1 Functional cloning and validation of TrkB as a suppressor of anoikis. **a**, Parental or Ras^{V12}-expressing RIE cells seeded into ULC tissue culture plates and photographed at × 50 magnification after 3 days (top). The bottom panel shows subsequent transfer of the cells to adhesive tissue culture plates, followed by fixation and crystal violet staining 2 days later. **b**, Outline of the screen. See Methods for details. **c**, Suppression of anoikis by clone ME-3, relative to a GFP-control, photographed at ×50 (top) and ×1 (bottom) magnification and at indicated time points. **d**, RIE cells expressing cDNAs as indicated, seeded on adhesive plates and photographed at ×200 magnification. **e**, RIE cells expressing cDNAs as indicated, seeded into ULC plates and photographed in time at ×50 (day 3) and ×1 (day 14) magnification. **f**, Single cell suspensions of RIE cells expressing cDNAs as indicated, seeded into soft-agar and photographed at ×50 magnification 1 week later.

As anoikis is defined as apoptosis caused by lack of adhesion[2], we examined whether it was specifically apoptosis that was prevented by TrkB. First, staining with an apoptosis-dependent fluorescent dye (3,3′-dihexyloxa-carbocyanine iodide, $DiOC_6(3)$) showed that, in agreement with previous results[6,7], RIE cells underwent apoptosis upon attachment withdrawal (Fig. 2a, left). By contrast, apoptosis was completely blocked by TrkB (Fig. 2a, right). Second, we determined by immunoblotting the protein levels of cleaved caspase-3, a primary executioner of apoptosis. Whereas no activated caspase-3 was detected in any of the cell lines when grown on adhesive dishes, it was produced by control and BDNF-expressing cells when they were brought into suspension (Fig. 2b). By contrast, cleaved caspase-3 production was completely suppressed by TrkB, regardless of the presence of TrkB's ligand. Together, these results indicate that it is apoptosis, resulting from lack of adhesion, that is effectively suppressed by TrkB.

Integrins are principal mediators of adhesion between cells and extracellular matrix proteins, including fibronectin, and they transduce signals critically required for cell survival[16,17]. Therefore, we examined whether TrkB-mediated resistance to anoikis depends on fibronectin, or on any other potential survival factor(s) present in cell culture serum. When TrkB-expressing cells were deprived of serum, they were partially protected from apoptosis, relative to control cells (Fig. 2c). However, BDNF-stimulated TrkB rendered cells resistant to anoikis, despite the complete absence of serum. This effect was not due to a general pro-survival function of TrkB, as TrkB, in contrast to the anti-apoptotic Bcl-2 protein, completely failed to protect adherent c-Myc-expressing fibroblasts from apoptosis resulting from serum withdrawal (Fig. 2d, e). Therefore, in untransformed epithelial cells, the BDNF–TrkB axis generates a signal that is sufficiently potent to allow, in the absence of any exogenous

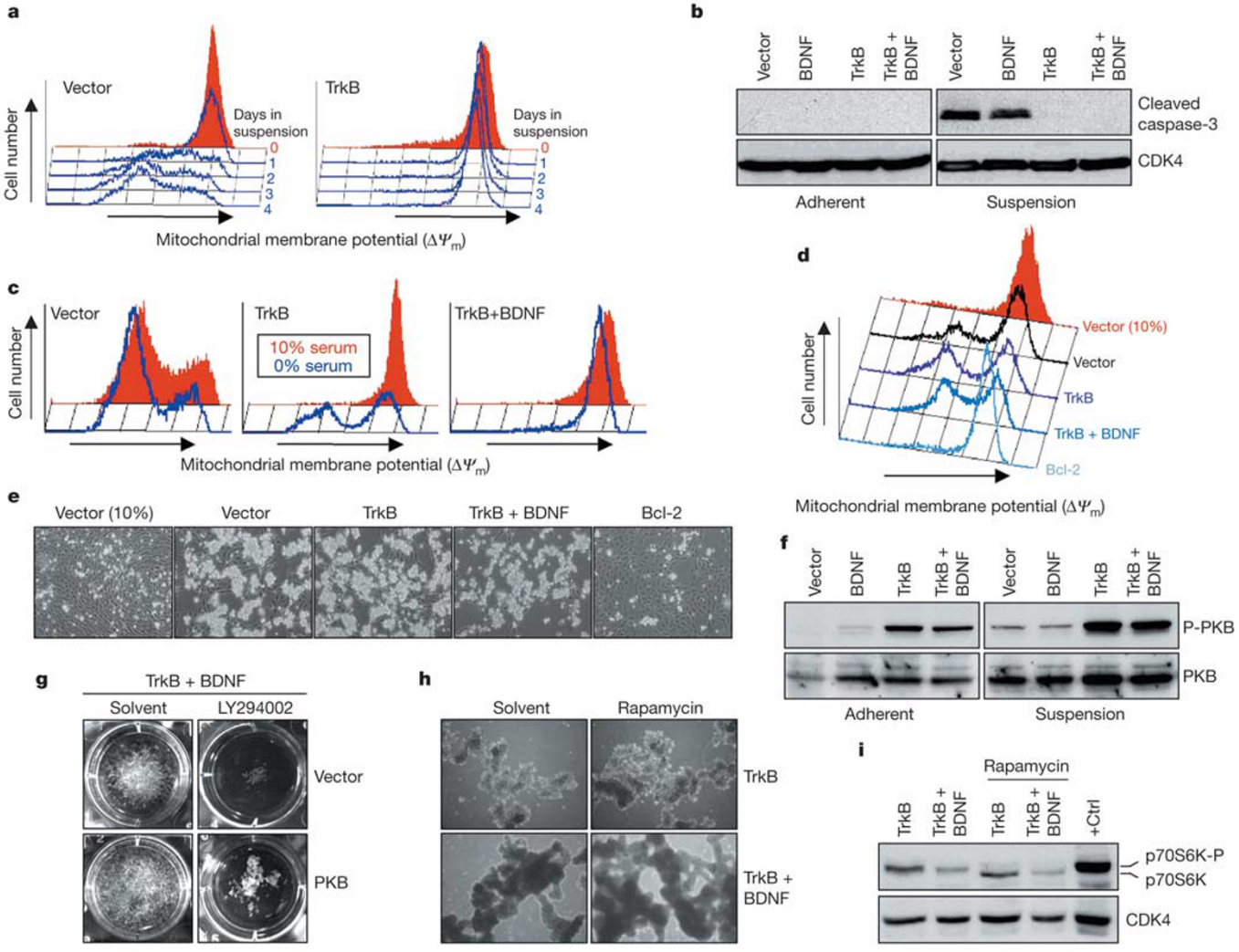

Figure 2 Specific suppression of anoikis-associated apoptosis by TrkB. **a**, Control or TrkB-expressing RIE cells seeded into ULC plates and analysed for apoptosis over time by DiOC6(3) staining for FACS analysis[30]. Right- and left-hand peaks reflect living and apoptotic cells respectively. **b**, Immunoblotting for cleaved caspase-3 of lysates from RIE cells expressing indicated cDNAs, on adhesive (left) or ULC (right) plates, for 2 days. CDK4 serves as loading control. **c**, RIE cells expressing indicated cDNAs, seeded either in the presence (red) or absence (blue) of serum into ULC plates and analysed for apoptosis 3 days later, as in **a**. Results with 0.1% serum were similar to those with 0% (not shown). **d**, **e**, Rat1 fibroblasts co-expressing c-Myc and indicated cDNAs, on adhesive dishes, in the absence of serum for 3 days and analysed by FACS (**d**) and photographed at ×200 magnification (**e**). Empty vector-transduced cells in 10% serum (Vector 10%) serve as control. **f**, Immunoblotting for serine 473-phosphorylated PKB (P-PKB) and total PKB of lysates from RIE cells expressing indicated cDNAs, on adhesive (left) or ULC plates (right) for 2 days. **g**, TrkB/BDNF co-expressing cells, either in the presence or absence of activated PKB, treated after spheroid formation with LY294002 (20 μM) or solvent and photographed 12 days later at ×1 magnification. **h**, **i**, TrkB/BDNF-expressing cells treated after spheroid formation with rapamycin (20 nM), photographed at ×50 magnification 2 days later (**h**) and subsequently used for immunoblotting for p70S6K and CDK4 as loading control (**i**). Similar results were obtained for 1-week treatment (not shown).

factors, survival in the face of a strong and specific pro-apoptotic anoikis signal.

To investigate whether TrkB directly activates survival signalling, as well as to identify its downstream targets, we first examined the potential involvement of protein kinase B (PKB; also known as AKT), which by itself is sufficient to suppress anoikis[18,19]. Under adherent conditions, TrkB induced production of activated, phosphorylated PKB (Fig. 2f, left). As TrkB/BDNF-expressing cells on adhesive dishes show diminished cell–cell interactions (Fig. 1d), this result demonstrates that, rather than through promoting cell–cell adhesion, TrkB directly activates the PKB survival pathway. This result, however, does not rule out the possibility that aggregate formation may contribute to survival signalling in suspension. Importantly, PKB activation was maintained in cells challenged with anoikis (Fig. 2f, right), raising the possibility that the PKB pathway mediates anoikis suppression by TrkB. Indeed, blocking PKB-dependent signalling by pharmacological inhibition of its major upstream regulator, phosphatidylinositol-3-OH kinase (PI(3)K), with LY294002 significantly interfered with TrkB-mediated survival (Fig. 2g; Supplementary Fig. S2a, b). In turn, cell death was prevented by activated PKB, excluding aspecific cytotoxic effects of LY294002, and further supporting a central role for PKB in anoikis suppression by TrkB. In line with previous data on Madine–Darby canine kidney (MDCK) cells[18], PI(3)K was also sufficient to suppress anoikis, albeit to a lesser degree than TrkB (Supplementary Fig. S2c). One of the critical downstream targets of the PI(3)K/PKB pathway is p70S6K, a kinase implicated both in anoikis and lymphomagenesis[18,20]. However, although rapamycin (a specific inhibitor of mTOR, which is a regulator of p70S6K) blocked p70S6K phosphorylation, it completely failed to affect the survival of TrkB-expressing cells in suspension (Fig. 2h, i). Similarly, dominant interference with signalling by Rac proteins (another target of PKB), or pharmacological inhibition of MEK did not prevent suppression of anoikis by TrkB (Supplementary Fig. S2d, e). We conclude that TrkB activates PI(3)K/PKB signalling, which contributes to anoikis resistance.

The main objective of this study was to assess the feasibility of using anoikis suppression as a basis to identify metastasis-inducing (onco)genes. When non-malignant cells expressing TrkB, either alone or in conjunction with its ligand, were introduced into nude mice, they rapidly formed tumours with high efficiencies, whereas vector and BDNF-expressing cells failed to do so (Supplementary Table S1). Therefore, expression of TrkB is sufficient to convert non-malignant epithelial cells into highly tumorigenic cells.

To address whether TrkB endows epithelial cells with metastatic potential as well, we first re-engineered our cell panel to express luciferase, which allows non-invasive *in vivo* imaging in live mice[21]. Each polyclonal cell line was administered intravenously to nude mice, and outgrowth and the location of tumours was monitored. Luciferase imaging showed that, although at 90 min after injection control cells were apparently viable and had accumulated in the lungs to at least the same extent as TrkB/BDNF co-expressing cells, no luciferase signal was detectable at 6 days (Fig. 3a). Indeed, control and BDNF-expressing cells failed to form tumours within 100 days after inoculation (Fig. 3b), consistent with the hypothesis that non-malignant epithelial cells fail to survive for a prolonged period in the absence of appropriate attachment[2]. By contrast, TrkB-expressing epithelial cells colonized the lungs and heart, where they formed rapidly growing tumours (Fig. 3c). This phenotype was even more pronounced for TrkB/BDNF-expressing cells, which caused metastases throughout the body (Fig. 3a, c; Supplementary Fig. S3). The cooperation between TrkB and BDNF in inducing metastasis therefore recapitulated their collaboration in suppressing anoikis under low-serum conditions (which may better approximate the situation *in vivo* than does 10% serum; compare Fig. 2c to Fig. 3c).

Microscopic pathological analysis showed the capacity of TrkB to induce solid, non-encapsulated tumours with undifferentiated properties (Fig. 4 and Supplementary Fig. S4). The tumours showed malignant cellular characteristics, including a high mitotic index, a high nucleus:cytoplasm ratio, and notable cellular and nuclear pleomorphism. TrkB-specific immunohistochemistry showed that these tumours were able to efficiently invade both blood and lymphatic vessels in various tissues, including liver, kidney, lung and heart (Fig. 4a–f, i, j and Supplementary Fig. S4). This infiltrative character of TrkB-driven tumours was also markedly illustrated by

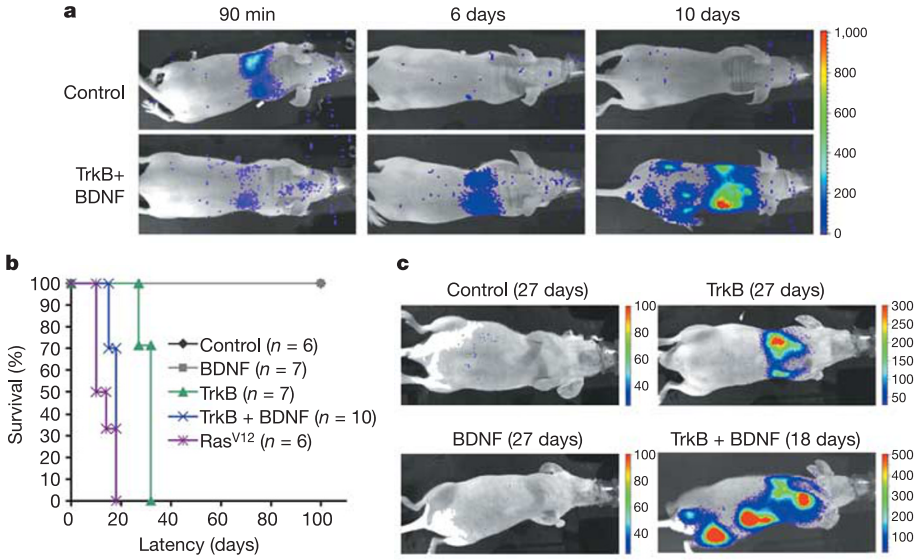

Figure 3 Tumorigenic potential of TrkB. **a**–**c**, Mice injected intravenously with RIE cells co-expressing a luciferase gene and indicated cDNAs, and subjected to *in vivo* imaging at indicated time points, with relative light units per pixel indicated in colour (**a**, **c**), or represented in a Kaplan–Meier survival plot (**b**). Note the relatively short latency of TrkB/BDNF-induced tumours and different imaging sensitivities used (**c**).

their capacity to destruct and invade bones (Supplementary Fig. S4g–i). Furthermore, these tumours, when present as large tumour masses, were viable and proliferating, as judged by their very low apoptotic and high proliferative indices respectively (Fig. 4 g, h, k). Importantly, this viable and non-apoptotic character was retained when these tumours extended into vessels (Fig. 4i, j), conceivably contributing to their metastatic potential and consistent with our finding *in vitro* that TrkB suppresses anoikis. The tumours were so invasive, destructive and fast-growing that only 18 days after administration, all mice had been euthanized (Fig. 3b, Supplementary Fig. S3).

As the intravenous metastasis system precludes an assessment of the early stages of metastasis (tissue invasion and endothelial or lymphatic intravasation by disseminated tumour cells), we also introduced TrkB/BDNF co-expressing cells subcutaneously. To increase the time window in which metastasis could occur, tumours that arose within a week were surgically removed, and upon relapse mice were killed. In agreement with, and extending the results described above, pathological examination showed that the subcutaneous tumour cells had efficiently infiltrated muscles, lymphatic vessels and regional lymph nodes, eventually causing several metastases at the pleural side of the lungs (Fig. 4l–p). Together, these results demonstrate that TrkB acts as a potent oncogene that converts non-malignant epithelial cells into metastasizing tumour cells.

TrkB and BDNF are frequently overexpressed in human cancer, including pancreatic and prostate carcinomas, Wilms' tumour and neuroblastomas, particularly those with aggressive behaviour and poor prognosis[22–25]. Moreover, recent sequence analysis of the tyrosine kinome in colorectal cancers has shown mutations within the kinase domain of TrkB[26]. Although these observations have associated TrkB with cancer, it has been unclear whether deregulated TrkB can act oncogenically. We find that TrkB generates a specific and potent pro-survival signal that renders epithelial cells resistant to anoikis. This is accompanied by the acquirement of potent tumorigenic, invasive and metastatic capacities, arguing that TrkB may directly contribute to human malignancies. Although our data are consistent with the hypothesis that suppression of anoikis contributes to the acquisition of a metastatic phenotype, other properties of TrkB, including induction of invasiveness, may contribute to its aggressive tumorigenic effects.

The propensity to metastasize may be determined by the gene

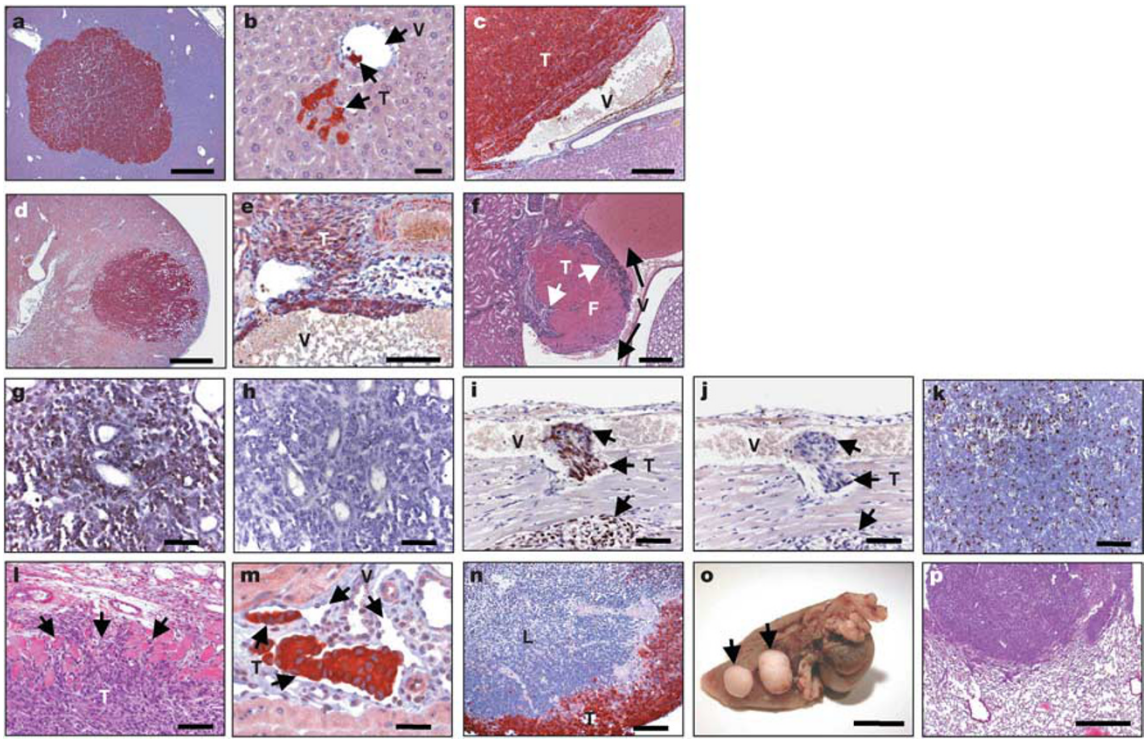

Figure 4 Metastatic potential of TrkB. **a**–**j**, Pathological characteristics of tumour processes after tail vein injection into nude mice. **a**, Large tumour nodule within liver. **b**, Clusters of tumour cells located in liver sinusoids and a tumour cell located in vena hepatica branch. **c**, Tumour nodule within liver, invading a vena portae branch. **d**, Large tumour within kidney. **e**, Detail of a renal tumour growing within lumen of large vein. **f**, Another plane of the section shown in **e**, demonstrating renal tumour extending into vein, activating the blood coagulation system and causing fibrin deposition (F). **g**, Detail of tumour in **d**, showing tumour cells located between renal tubules, and high proliferative index, as evident from nuclear MCM7 immunoreactivity. **h**, Representative photomicrograph of section in **g**, showing lack of apoptosis, as evident from absence of cleaved caspase-3 immunoreactivity. **i**, Tumour nodule (with edge of large tumour mass at bottom side of microphotograph), spreading into branch of coronary vein of the myocardium and showing high proliferative index, as evident from MCM7 immunopositivity. **j**, Representative photomicrograph of adjacent section of **i**, showing lack of apoptosis of tumour cells infiltrating coronary vein, as evidenced by a lack of expression of cleaved caspase-3. **k**, Splenic lymphoma from an unrelated mouse, showing numerous apoptotic cells, serving as positive control for cleaved caspase-3-specific immunohistochemistry. **l**–**p**, Pathological characteristics of tumour processes upon subcutaneous injection. Representative microphotographs showing the metastatic process in one mouse. **l**, Subcutaneously injected tumour cells infiltrating muscle tissue (arrows). **m**, Clusters of tumour cells infiltrating lymphatic vessels, at a distance from the subcutaneous tumour. **n**, Tumour infiltrating axillary lymph node (L) draining the tumour site. **o**, Large metastases at pleural side of the lungs (apical lobe of the right lung was removed to allow a better view of the tumour nodules). **p**, One of the metastases shown in **o**. Immunohistochemistry was performed for TrkB (**a**–**e**, **m**, **n**), MCM7 (**g**, **i**), or cleaved caspase-3 (**h**, **j**, **k**). **f**, **l**, **p**, Haematoxylin and eosin stainings. T and V mark tumours and vessels, respectively. Scale bars: 500 μm (**a**, **p**); 200 μm (**c**, **e**); 100 μm (**f**, **k**, **l**, **n**); 50 μm (**b**, **g**–**j**); 20 μm (**m**); 1 mm (**d**); 5 mm (**o**). Rows indicate four individual sets of photographs.

expression signature already present in the primary tumour[27]. The results presented here raise the possibility that TrkB activation may represent such an early event during multistep tumorigenesis, endowing primary cells with a wide spectrum of capacities contributing to cancer. Mainly on the basis of the overexpression of TrkB in poor-prognosis human tumours, pan-Trk-inactivating drugs are already being developed[28]. Our findings predict that drug-mediated inactivation of specifically TrkB may have a notable impact on the tumorigenic and metastatic capacities of human tumours with overexpressed or mutated TrkB. Finally, our results not only illustrate the feasibility of using anoikis suppression as a functional property to identify metastasis-associated oncogenes, but also show its potential use in high-throughput screens for TrkB-inhibitory cancer therapeutics. □

Methods

Genome-wide retroviral cDNA screen

RIE cells were infected, in the presence of 5 μg ml^{-1} polybrene, with a high-complexity retroviral pEYK cDNA library[8], prepared from a whole mouse embryo and propagated in Phoenix packaging cells as eight pools representing two size fractions (1–3 and >3 kilobases (kb)). Filtered (0.45 μm) viral supernatant pools representing the two size fractions were used to infect 0.75×10^6 cells each, and 2 days later, cells were collected by trypsinization and transferred to four ULC six-well cell culture dishes (Costar) in total. After 6 days, cells were transferred back to regular, adhesive tissue culture dishes, to allow anoikis-resistant cells to expand. After 10 days, cells were re-challenged with an anoikis insult, by transferring them into ULC plates. One week later, surviving colonies were isolated and transferred to 24-well adhesive plates, and allowed to expand. Then, genomic DNA was isolated and digested with either *Not*I or *Asc*I, re-ligated and transformed into *Escherichia coli*. Plasmid DNA was isolated and transfected onto Phoenix cells. Virus supernatant was subsequently used to infect fresh RIE cells and a second-round screen was performed to validate the biological activity of the respective proviral cDNAs. Finally, proviral cDNA inserts were isolated from positive clones, shuttled and analysed by DNA sequencing. One of the anoikis-resistant clones (ME-3) contained a wild-type, full-length murine cDNA encoding TrkB, which was sub-cloned into the pBabe-puro retroviral vector. Of the 24 wells screened, 12 contained anoikis-resistant clones, sometimes several per well, giving 20 anoikis-resistant clones in total. Polymerase chain reaction (PCR) analysis for retroviral TrkB inserts showed that, in addition to ME-3, TrkB was present in seven clones (derived from four different wells). The remaining 13 clones remain to be analysed further.

A murine full-length cDNA encoding BDNF was isolated from a mouse cDNA library (Clontech) by PCR (primers available upon request), and sub-cloned into the pBabe-hygro retroviral vector.

Cell culture and *in vitro* assays

RIE cells were maintained in high-glucose Dulbecco's modified Eagle's Medium (DMEM) (Life Technologies) supplemented with 9% fetal bovine serum (PAA Laboratories) and antibiotics. c-Myc-expressing Rat1 fibroblasts were provided by K. Berns. Phoenix packaging cells were used to generate ecotropic retroviruses, as described[29]. In general, a single-infection round of 6 h was sufficient to infect at least 90% of the population. RIE cells were infected with pBabe retroviral vectors carrying selectable markers and cDNA inserts, and at 1 to 2 days post infection selected with puromycin (1.5 μg ml^{-1}) or hygromycin (75 μg ml^{-1}) for at least 5 days. After confirming that all mock-infected cells were dead, the cells were used in various assays.

Proliferation curves were performed with two independent cultures for each cell line, and data points were collected in triplicate, as described[29].

To determine the cloning efficiency of RIE cell lines in semi-solid medium, soft agar assays were performed, as described[29].

To measure apoptosis, cells were collected from either adhesive or suspension plates (both populations were subjected to trypsinization), treated with $DiOC_6(3)$ (a fluorescing dye that accumulates in mitochondria as a function of membrane potential[30]; Molecular Probes) in PBS for 15 min at 37 °C, and subsequently analysed by fluorescence-activated cell sorting (FACS).

Pharmacological inhibition was performed with LY294002 (20 μM), PD98059 (20 μM), K-252A (300 nM) or rapamycin (20 nM), all from Calbiochem. Retroviral vectors encoding myristylated PKB and activated p110-CAAX PI(3)K were gifts from F. Scheeren and J. Collard respectively.

Immunohistochemistry

Paraffin-embedded tissue was cut into 4-μm sections, deparaffinized and rehydrated. Upon antigen retrieval performed with citrate buffer (pH, 6) and incubation with primary and secondary antibodies, immunocomplexes were detected with either DAB/H2O2 or AEC (Dakocytomation).

Antibodies

For western blotting and immunohistochemistry, the following antibodies were used: MS-862 for MCM-7 (NeoMarkers); AC-74 for actin (Sigma); 9661 for cleaved caspase-3 and 9202 for p70S6K (Cell Signalling); SC-8316 for TrkB, SC-260 for CDK4, SC-7985 for Ser 473-phosphorylated PKB and SC-8312 for PKB (all Santa Cruz).

In vivo assays

To determine tumorigenicity and metastatic potential, the RIE cell panel (1×10^6 cells) was injected subcutaneously into athymic nude mice in each flank. Mice were inspected daily and were killed at the time tumours reached a diameter of 10 mm.

To measure metastatic potential and allow *in-vivo* bioluminescence luciferase imaging, mice were injected intravenously with the RIE cell panel (1×10^6 for Fig. 3b, c, and 3×10^6 for Fig. 3a; administration of 10^7 cells gave identical results; not shown), co-expressing a luciferase gene and cDNAs of interest. *In vivo* bioluminescence imaging of luciferase expression was performed as described[21]. Generally, for each cell line, 2–4 mice were imaged in time, with similar results.

Received 27 April; accepted 16 June 2004; doi:10.1038/nature02765.

1. Frisch, S. M. & Ruoslahti, E. Integrins and anoikis. *Curr. Opin. Cell Biol.* **9,** 701–706 (1997).
2. Frisch, S. M. & Screaton, R. A. Anoikis mechanisms. *Curr. Opin. Cell Biol.* **13,** 555–562 (2001).
3. Hanahan, D. & Weinberg, R. A. The hallmarks of cancer. *Cell* **100,** 57–70 (2000).
4. Klein, R., Parada, L. F., Coulier, F. & Barbacid, M. trkB, a novel tyrosine protein kinase receptor expressed during mouse neural development. *EMBO J.* **8,** 3701–3709 (1989).
5. Huang, E. J. & Reichardt, L. F. Trk receptors: roles in neuronal signal transduction. *Annu. Rev. Biochem.* **72,** 609–642 (2003).
6. Shao, J., Sheng, H., DuBois, R. N. & Beauchamp, R. D. Oncogenic Ras-mediated cell growth arrest and apoptosis are associated with increased ubiquitin-dependent cyclin D1 degradation. *J. Biol. Chem.* **275,** 22916–22924 (2000).
7. McFall, A. *et al.* Oncogenic Ras blocks anoikis by activation of a novel effector pathway independent of phosphatidylinositol 3-kinase. *Mol. Cell Biol.* **21,** 5488–5499 (2001).
8. Koh, E. Y., Chen, T. & Daley, G. Q. Novel retroviral vectors to facilitate expression screens in mammalian cells. *Nucleic Acids Res.* **30,** e142 (2002).
9. Glass, D. J. *et al.* TrkB mediates BDNF/NT-3-dependent survival and proliferation in fibroblasts lacking the low affinity NGF receptor. *Cell* **66,** 405–413 (1991).
10. Jaboin, J., Hong, A., Kim, C. J. & Thiele, C. J. Cisplatin-induced cytotoxicity is blocked by brain-derived neurotrophic factor activation of TrkB signal transduction path in neuroblastoma. *Cancer Lett.* **193,** 109–114 (2003).
11. Ho, R. *et al.* Resistance to chemotherapy mediated by TrkB in neuroblastomas. *Cancer Res.* **62,** 6462–6466 (2002).
12. Klein, R. *et al.* Targeted disruption of the trkB neurotrophin receptor gene results in nervous system lesions and neonatal death. *Cell* **75,** 113–122 (1993).
13. Banks, G. B. & Noakes, P. G. Elucidating the molecular mechanisms that underlie the target control of motoneuron death. *Int. J. Dev. Biol.* **46,** 551–558 (2002).
14. Soppet, D. *et al.* The neurotrophic factors brain-derived neurotrophic factor and neurotrophin-3 are ligands for the trkB tyrosine kinase receptor. *Cell* **65,** 895–903 (1991).
15. Squinto, S. P. *et al.* trkB encodes a functional receptor for brain-derived neurotrophic factor and neurotrophin-3 but not nerve growth factor. *Cell* **65,** 885–893 (1991).
16. Ruoslahti, E. & Vaheri, A. Cell-to-cell contact and extracellular matrix. *Curr. Opin. Cell Biol.* **9,** 605–607 (1997).
17. Reginato, M. J. *et al.* Integrins and EGFR coordinately regulate the pro-apoptotic protein Bim to prevent anoikis. *Nature Cell Biol.* **5,** 733–740 (2003).
18. Khwaja, A., Rodriguez-Viciana, P., Wennstrom, S., Warne, P. H. & Downward, J. Matrix adhesion and Ras transformation both activate a phosphoinositide 3-OH kinase and protein kinase B/Akt cellular survival pathway. *EMBO J.* **16,** 2783–2793 (1997).
19. Schmidt, M., Hovelmann, S. & Beckers, T. L. A novel form of constitutively active farnesylated Akt1 prevents mammary epithelial cells from anoikis and suppresses chemotherapy-induced apoptosis. *Br. J. Cancer* **87,** 924–932 (2002).
20. Wendel, H. G. *et al.* Survival signalling by Akt and eIF4E in oncogenesis and cancer therapy. *Nature* **428,** 332–337 (2004).
21. Vooijs, M., Jonkers, J., Lyons, S. & Berns, A. Noninvasive imaging of spontaneous retinoblastoma pathway-dependent tumours in mice. *Cancer Res.* **62,** 1862–1867 (2002).
22. Nakagawara, A., Azar, C. G., Scavarda, N. J. & Brodeur, G. M. Expression and function of TRK-B and BDNF in human neuroblastomas. *Mol. Cell Biol.* **14,** 759–767 (1994).
23. Aoyama, M. *et al.* Human neuroblastomas with unfavorable biologies express high levels of brain-derived neurotrophic factor mRNA and a variety of its variants. *Cancer Lett.* **164,** 51–60 (2001).
24. Eggert, A. *et al.* Expression of the neurotrophin receptor TrkB is associated with unfavorable outcome in Wilms' tumor. *J. Clin. Oncol.* **19,** 689–696 (2001).
25. Brodeur, G. M. Neuroblastoma: biological insights into a clinical enigma. *Nature Rev. Cancer* **3,** 203–216 (2003).
26. Bardelli, A. *et al.* Mutational analysis of the tyrosine kinome in colorectal cancers. *Science* **300,** 949 (2003).
27. Bernards, R. & Weinberg, R. A. A progression puzzle. *Nature* **418,** 823 (2002).
28. Ruggeri, B. A., Miknyoczki, S. J., Singh, J. & Hudkins, R. L. Role of neurotrophin-trk interactions in oncology: the anti-tumor efficacy of potent and selective trk tyrosine kinase inhibitors in pre-clinical tumor models. *Curr. Med. Chem.* **6,** 845–857 (1999).
29. Peeper, D. S. *et al.* A functional screen identifies hDRIL1 as an oncogene that rescues RAS-induced senescence. *Nature Cell Biol.* **4,** 148–153 (2002).
30. Zamzami, N. *et al.* Mitochondrial control of nuclear apoptosis. *J. Exp. Med.* **183,** 1533–1544 (1996).

Supplementary Information accompanies the paper on **www.nature.com/nature**.

Acknowledgements We thank M. van der Valk and J.-Y. Song for help with animal pathology and experiments; E. Mesman, J. Bulthuis, K. de Goeij and M. Tjin-a-Koeng for histotechnical analysis; and L. Rijswijk, F. van der Ahé, H. Grimminck and L. Tolkamp for help with oncogenicity experiments and animal husbandry. We thank E. Koh and G. Daley for providing pEYK libraries; R. Beauchamp for RIE cells; K. Berns, B. Burgering, E. Danen, R. van der Kammen, R. Kortlever, S. Lens, F. Scheeren, S. Tait, E. de Vries and A. Werner for various reagents; R. Bernards, J. Borst, J. Collard, J. Hilkens, W. Mooi, E. Roos, A. Sonnenberg, as well as the members of our laboratory and division, for helpful discussions; and M. van Lohuizen and A. Berns for suggestions and critical reading of the manuscript. D.S.P. and T.L. were supported by the Netherlands Organization for Scientific Research (NWO).

Competing interests statement The authors declare that they have no competing financial interests.

Correspondence and requests for materials should be addressed to D.S.P. (d.peeper@nki.nl).

Argos inhibits epidermal growth factor receptor signalling by ligand sequestration

Daryl E. Klein[1]*, Valerie M. Nappi[1]*, Gregory T. Reeves[2], Stanislav Y. Shvartsman[2] & Mark A. Lemmon[1]

[1]*Department of Biochemistry and Biophysics, University of Pennsylvania School of Medicine, 809C Stellar-Chance Laboratories, 422 Curie Boulevard, Philadelphia, Pennsylvania 19104-6059, USA*
[2]*Department of Chemical Engineering and the Lewis-Sigler Institute for Integrative Genomics, Princeton University, Carl Icahn Laboratory, Washington Road, Princeton, New Jersey 08544, USA*

* These authors contributed equally to this work

The epidermal growth factor receptor (EGFR) has critical functions in development and in many human cancers[1–3]. During development, the spatial extent of EGFR signalling is regulated by feedback loops comprising both well-understood activators and less well-characterized inhibitors[3,4]. In *Drosophila melanogaster* the secreted protein Argos functions as the only known extracellular inhibitor of EGFR[5], with clearly identified roles in multiple stages of development[3]. Argos is only expressed when the *Drosophila* EGFR (DER) is activated at high levels[6], and downregulates further DER signalling. Although there is ample genetic evidence that Argos inhibits DER activation, the biochemical mechanism has not been established. Here we show that Argos inhibits DER signalling without interacting directly with the receptor, but instead by sequestering the DER-activating ligand Spitz. Argos binds tightly to the EGF motif of Spitz and forms a 1:1 (Spitz:Argos) complex that does not bind DER *in vitro* or at the cell surface. Our results provide an insight into the mechanism of Argos function, and suggest new strategies for EGFR inhibitor design.

Argos is a secreted *Drosophila* protein comprising 444 amino acids that has an atypical EGF-like motif at its carboxy terminus[7]. Argos was genetically identified as an inhibitor of DER signalling[6–8]. Its expression is induced by DER activation[5,6], constituting a negative feedback mechanism that is involved in more than ten distinct DER-dependent processes during *Drosophila* development[3]. Several reports have argued that Argos interacts directly with DER to inhibit its signalling[5,9,10], leading us to hypothesize that Argos stabilizes an autoinhibited receptor configuration such as that revealed in our recent crystallographic studies of human EGFR[11].

To investigate how Argos inhibits DER signalling, we purified recombinant secreted Argos, Spitz (a TGFα-like DER-activating ligand[3]) and the DER2 extracellular region (sDER2) from transfected *Drosophila Schneider*-2 (S2) cells. Contrary to our expectations, sDER2 completely failed to interact with immobilized Argos in surface plasmon resonance (SPR) studies (Fig. 1a). Unexpectedly, Spitz bound to the same immobilized Argos with high affinity (Fig. 1a). These observations were not artefacts of Argos immobilization, as soluble Argos also bound strongly to immobilized Spitz ($K_d = 20 \pm 3$ nM) and did not bind to immobilized sDER2 (Fig. 1b). As shown in Fig. 1b and 1c, immobilized Spitz binds ~tenfold more strongly to Argos than to sDER2 (K_d for Spitz binding by sDER2 was 157 ± 37 nM, compared with 132 nM for EGF binding by human sEGFR[11]). Furthermore analytical ultracentrifugation experiments showed that Argos and Spitz form a (monomeric) 1:1 complex in solution (Fig. 1d), and that Spitz induces the expected sDER2 dimerization (Fig. 1e). Thus, SPR and analytical ultracentrifugation experiments demonstrate that Argos binds directly to the activating ligand Spitz (and not to DER itself), in direct contrast to what was previously suggested from less quantitative studies[5,9,10]. As shown in Supplementary Fig. S1, we identified the Argos binding site as the EGF-like domain of Spitz (residues 78–141), and found that Spitz binds to the C-terminal 220 amino acids of Argos, consistent with the ability of this Argos fragment to rescue loss-of-function alleles *in vivo*[12].

Because Argos and DER both bind the EGF-like domain of Spitz, we hypothesized that they may compete with one another for the same binding site on Spitz. Argos could thus 'sequester' Spitz away from DER by blocking the receptor-binding site on the activating ligand. This model has precedents in insulin-like growth factor (IGF)-binding proteins[13] and bone morphogenetic protein (BMP) antagonists[14], which both sequester their target ligands in this way. To test this hypothesis, we analysed the effect of added Argos on Spitz binding to immobilized sDER2 (Fig. 2a). On its own, Spitz (at 250 nM) bound immobilized sDER2 to give an SPR binding signal of ~600 response units (RUs). The addition of increasing amounts of Argos (to a fixed Spitz concentration) progressively reduced this signal until it reached zero, when Argos was present in slight excess (≥1.1-fold). Because binding of either Spitz or Argos to immobilized sDER2 would contribute to the SPR signal, these results can only be explained if Argos binds directly to Spitz in solution (and not at all to immobilized sDER2), and thus blocks Spitz binding to the receptor. The finding that sDER2 binding is abolished when Argos and Spitz are approximately equimolar (performed at 12 times K_d for the Argos–Spitz interaction) is consistent with the 1:1 (Argos:Spitz) stoichiometry measured in Fig. 1d. We therefore conclude that Argos can act as a ligand 'sink' that efficiently sequesters Spitz in an inactive 1:1 complex and prevents Spitz from binding its receptor.

We next investigated whether Argos can act as a ligand sink in a cellular context. Addition of Spitz at 10 nM, 50 nM or 100 nM induces robust tyrosine autophosphorylation of DER2 expressed in S2 cells (Fig. 2b), and this is progressively inhibited by increasing amounts of Argos. As expected if Argos inhibits DER signalling by sequestering Spitz into an inactive complex, when more Spitz is present in Fig. 2b, more Argos is required to prevent it all from receptor binding. The requirement for a larger excess of Argos over Spitz (~fivefold) in this experiment compared with Fig. 2a suggests that Spitz binds more strongly to cell surface DER2 than to immobilized sDER2 (this is known to be true in the human EGF system[15]).

To visualize Spitz and Argos at the cell surface, we labelled recombinant proteins with Alexa Fluor-488 and -633 respectively, using the same chemistry as employed for SPR immobilization. As shown in Fig. 2c, fluorescently labelled Spitz–488 was seen clearly at the plasma membrane (and in compartments likely to represent endosomes) in ~40% of living D2f cells (approximately 50% of D2f cells expressed DER2 when analysed by FACS), but was not seen in parental S2 cells (that do not express DER). In contrast, fluorescent Argos–633 showed no DER-dependent binding to the cell surface.